Sigma-Point Unscented Kalman Filter Used For AUV Navigation

Matko Barisic, Antonio Vasilijevic and Dula Nad

Abstract— **This paper presents an implementation of the Sigma-point Unscented Kalman Filter (SP-UKF) used in the simulated task of open-water navigation of two types of AUV. The first simulated vehicle is a large cruise-type vehicle modeled after the Instituto Superior Tecnico, Lisbon vehicle Infante. The second is a small, almost fully actuated vehicle with tunnel thrusters modeled after the SSC Pacific, San Diego vehicle CETUS II. The SP-UKF shows itself, after properly taking care of implementation details, to be a robust methodology which allows for efficient and correct navigation, aided by several typical sensors (DVL, USBL hydroacoustic localization systems, AHRS). The influence of currents on the navigation, and the ability of estimating the current components is also researched. The navigation fix is fed back to the low-level control loops aboard each vehicles to achieve sane and rational navigation of the waterspace that follows stably and robustly the command signals.**

I. INTRODUCTION

The problem of navigation of the underwater vehicles, although present in the technical and scientific community for a long time, is still a challenging one. Rather than the fundamental concepts, which have been systematically researched, the current focus is on using cheap sensor, modular embedded sensing and computing architectures and components, and robust, stochastically sound algorithms. As the autonomous underwater vehicles (AUV) market moves towards maturity [4], and off-the-shelf systems proliferate on the market, well engineered, stable and robust navigation filters continue to be more and more sought after.

This paper presents the use of a stochastically powerful filter built on the Kalman framework [13], [12], [26], introduced by van der Merwe [24], the *Sigma-point Unscented Kalman filter*, for the navigation of two different types of AUVs, both of whom are representative of today's off-the-shelf and in-house built systems operating in the Ocean. It is assumed that the vehicles are equipped with modern, MEMS-based strap-down AHRS[1] such as [15] for measuring the quaternions and/or Euler angle expressions of the vehicle attitude, down-market DVLs[2], such as [23] and an inverted USBL[3] hydroacoustic positioning system [25], [18] that features a vehicle-mounted transducer and a GPS-ground-truthed transponder suspended in the water column.

In section II, the basic information flow, and the block diagram of the employed variant of the Unscented Kalman filter are presented. Furthermore, it contains the description of several preprocessing procedures developed in [2] that significantly increase the robustness of navigation in real-world conditions. Section III contains the model dynamics of the two vehicles, whose response to navigation by way of low-level controllers for helm speed, heave speed, heading and/or pitch angle (depending on the vehicle type) fed back from the navigation filter will be researched. Section IV contains the low-level controllers used in the navigation simulation studies and the noise generation scheme employed to simulate realistic and non-stationary process and measurement noises. Ultimately, with all of these blocks fundamental in providing a realistic simulation framework, section V displays the results garnered from the simulation studies of the two vehicle dynamics. Section VI concludes the paper.

II. THE UNSCENTED KALMAN FILTER

The theory and the feasibility concept of the use of the *Unscented Kalman Filter* (UKF) is carried out in [24]. The UKF works with a cloud of points, each of which represents a *state hypothesis* embedded in the state-space spanned by the estimated variables, $\hat{\boldsymbol{\chi}}(k|k-1)$. These points are called *sigma-points* since they represent the $\pm 1\sigma$ deviations from the ex post mean estimate of the previous sample-time, $\hat{\boldsymbol{\chi}}(k-1|k-1)$ in the directions provided by the columns of the matrix square root of the process noise covariance matrix $\mathbf{P}_{\boldsymbol{\chi}}(k-1)$. Every hypotheses thus generated is propagated through the model dynamics of the estimated system, and the final product of the *prediction step*, $\hat{\boldsymbol{\chi}}(k|k-1)$ is a result of the weighted sum of the propagated hypotheses. The ex ante covariance matrix of the estimate, $\mathbf{P}_{\boldsymbol{\chi}}(k|k-1)$ is calculated on the basis of the deviations of the propagated hypotheses from $\hat{\boldsymbol{\chi}}(k|k-1)$.

The *correction cycle* is performed on the generation of a distinct set of *output hypotheses* in much the same way as the state hypotheses of the prediction step. Here, the sigma-points are determined by the columns of the matrix square root of the *measurement noise* covariance matrix, $\mathbf{R}_{\mathbf{v}}$, w.r.t. the ex ante estimate (i.e. pure prediction) $\hat{\boldsymbol{\chi}}(k|k-1)$. These hypotheses are propagated through the output model, which in the case of AUVs is the model kinematics, to obtain a propagated hypotheses cloud $\hat{\mathbf{y}}(k|k-1)$.

Calculating the statistics of the propagated output hypotheses and the cross-covariance between the propagated output and state hypotheses yields $\mathbf{P}_{\mathbf{y}}$, $\mathbf{P}_{\chi\mathbf{y}}$ which in turn are used

This research was made possible by the EU 2008-1-REGPOT grant for the "Developing the Croatian Underwater Robotics Research Potential" project, grant agreement no. 229553, and by the non-government organization Center for Underwater Systems and Technologies (CUST).

All authors are with the University of Zagreb, Faculty of Electrical Engineering and Computing, Laboratory for Underwater Systems and Technologies, Unska 3, HR-10000 Zagreb, Croatia. {matko.barisic, antonio.vasilijevic, dula.nad}@fer.hr

[1]Attitude and heading reference unit.

[2]Doppler velocity logger.

[3]Ultra-short baseline.

to derive the *Kalman gain matrix* $\mathbf{K}(k)$. As in any Kalman filter, the Kalman gain is used to (i) correct the ex ante mean $\hat{\boldsymbol{\chi}}(k|k-1)$ (the prediction) with the residual of the measurement $\mathbf{y}(k) - \hat{\mathbf{y}}(k|k-1)$, and (ii) to "tighten" the spectral radius of the ex post covariance matrix of the state estimates $\mathbf{P}_{\chi}(k|k)$ at sample-time k w.r.t. the ex ante value $\mathbf{P}_{\chi}(k|k-1)$ obtained from the statistics of the propagated state hypotheses.

The pseudo-code of the filter algorithm, as well as the parameters used in the initialization are given in [2].

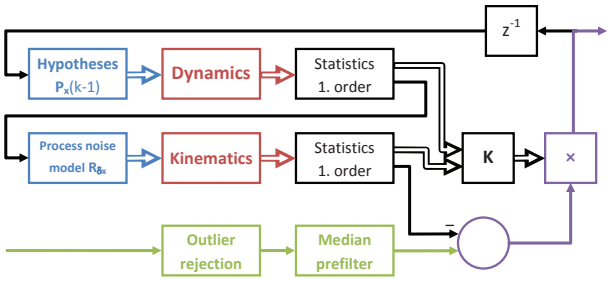

Fig. 1. Sigma-point Scaled Unscented Transform Kalman filter – SP-UKF.

From a practical point of view, the proposed filter needs to be robust to non-stationary, realistic noise, including flicker, bias, and nonlinearities, in all input, i.e. measurement channels. It needs to be robust to outliers, i.e. the navigation fix that it provides must not be influenced by manifestly and blatantly erroneous readings on any of the measurement channels. Ultimately, it needs to be robust to intermittent and sporadic failures to measure any single quantity among the input measurements. There needs to be some measure of interpolation available to the navigation filter. In order to address all of these issues, the final realization of the SP-UKF proposed in this paper features an outlier detector (and eliminator) and an interpolating median prefilter.

A. Outlier Rejector

The nature of the procedures used to identify the model dynamics of the two considered vehicles in [7], [22], low-level controller design and various undetermined operational conditions in nature contribute to significant *process noise*. Additionally, the nature of the navigation sensors – the AHRS, the hydroacoustic positioning system and the DVL, produces non-stationary, non-ergodic *measurement noise* with bias, non-linear effects, flicker and various other artifacts appears superimposed on the ground-truthed information. The combination of these two fundamental types of noises allows for large *outlier* measurements to be sporadically generated. To remedy their influence on the navigation fix, an algorithm must be implemented for their rejection prior to the input into the UKF.

Implementation-wise the SP-UKF deals with rejected outliers by overwriting the appropriate row of the measurement column vector $\mathbf{y}$ with `NaN`.

Outlier rows of $\mathbf{y}$ are considered those for which *any* values, inspected column-wise, fulfill:

$$\mathbf{R}_y(k) = \mathbf{y}(k)^{\mathrm{T}} \cdot \mathbf{y}(k) = \left[r_y^{(i,j)} \right] \quad (1)$$

$$i_{out} = \left\{ \arg_i \left(\exists j,\, r_y^{(i,j)} > 16 \cdot \mathbf{P}_{\boldsymbol{\chi}}(k) \right) \right\} \quad (2)$$

$$\mathbf{y}\left[\{i_{out}\}\right] \leftarrow \texttt{NaN} \quad (3)$$

Where $\mathbf{P}_{\boldsymbol{\chi}}(k)$ is the ex post covariance matrix of the estimate of the full-state vector returned by the SP-UKF at time k.

B. Interpolating Median Prefilter

A progression of `NaN` values, generated either by the sporadic and intermittent failures of the navigation sensors, or by the action of the outlier rejector, can destabilize the navigation filter and cause divergent control of a vehicle. To alleviate this concern, a *prefilter bank* designed in [2] is inserted previous to inputting data into the SP-UKF algorithm described above, and after the outliers have been rejected. The prefilter bank consists of order 5 1D median prefilters with interpolation capabilities for all measurement channels.

The prefilter algorithm functions in two distinct steps:

1) Replace `NaN` values from the local storage with interpolated values,
2) Return the median value from the local storage.

Linear interpolation is used to overwrite `NaN` values based on at least 2 valid measurements from among 5 stored samples retained at any sampling period.

III. AUV MODEL DYNAMICS

In this section, two significantly different AUVs are presented. Each of them is a separate and unique challenge for navigation. Their model dynamics and kinematics, as well as different low-level controllers are used in the simulated experiments to establish the quality of navigation achieved with the UKF.

The model dynamics of both vehicle utilize the dynamic states $\mathbf{x} \in \mathbb{R}^6$ from among $\boldsymbol{\chi} \in \mathbb{R}^{12}$, the full dynamic and kinematic state of a rigid body, defined as $\boldsymbol{\chi} = [\mathbf{x}^{\mathrm{T}} \quad \mathbf{z}^{\mathrm{T}}]^{\mathrm{T}} = [[\boldsymbol{u}^{\mathrm{T}} \quad \boldsymbol{\omega}^{\mathrm{T}}] \quad [\boldsymbol{x}^{\mathrm{T}} \quad \boldsymbol{\Theta}^{\mathrm{T}}]]^{\mathrm{T}} = [[[u\ v\ w]\ [p\ q\ r]]\ [[x\ y\ z]\ [\phi\ \theta\ \psi]]]^{\mathrm{T}}$, consisting of the concatenated states of the surge, sway and heave translational speeds of the vehicle, the rolling, pitching and yawing rates (angular speeds), the 3D position in the Earth-fixed frame of reference $\boldsymbol{x}$ and the attitude $\boldsymbol{\Theta}$ expressed in Euler angles of roll, pitch and yaw, respectively. The model dynamics are expressed in terms of an open-form or implicit second order non-linear differential equation in $\mathbf{x}$ for both vehicles, or broken up into six open-form or implicit second order non-linear differential equations according to the degrees of freedoms denoted $\{X, Y, Z, K, M, N\}$ for surge, sway, heave, roll, pitch and yaw, respectively.

Some standard terms occurring in both models are the dimension-less coefficients expressed as $[A]_{[b]}$, where $A \in \{X, Y, Z, K, M, N\}$ signifies the degree of freedom and b states the terms that the coefficient multiplies to produce a

contribution to the force or torque. Furthermore the mass-inertia tensor $\mathbf{M} \in \mathbb{R}^{6\times 6}$ is assumed for both vehicles to be of the form:

$$\mathbf{M} = \text{diag}\{[\ m \quad m \quad m \ \mid\ \mathbf{I}\ ]\} \tag{4}$$

$$\mathbf{I} = \begin{bmatrix} I_x & I_{xy} & I_{zx} \\ I_{xy} & I_y & I_{yz} \\ I_{zx} & I_{yz} & I_z \end{bmatrix} \tag{5}$$

Finally, the meta-centric restoring forces due to gravity, $\mathbf{g}$, are of the same form for both vehicles:

$$\mathbf{g} = \begin{bmatrix} (mg - B)\sin\theta \\ -(mg - B)\cos\theta\sin\phi \\ -(mg - B)\cos\theta\cos\phi \\ -(y_G mg - y_B B)\cos\theta\cos\phi + (z_G mg - z_B B)\cos\theta\sin\phi \\ (x_G mg - x_B B)\cos\theta\cos\phi + (z_G mg - z_B B)\sin\theta \\ -(x_G mg - x_B B)\cos\theta\sin\phi - (y_G mg - y_B B)\sin\theta \end{bmatrix} \tag{6}$$

Where:
- m is the mass of the vehicle,
- g is the acceleration due to gravity,
- B is the positive buoyancy, i.e. the force of the hydrostatic lift on the vehicle generated by the displacement,
- $\boldsymbol{x}_G = [x_G \quad y_G \quad z_G]^{\mathrm{T}}$ is the vector of the offset of the center of gravity from the origin of the body-fixed frame of reference wherein the differential equations of the model dynamics are expressed, $\boldsymbol{x}_G \overset{\text{id}}{=} \boldsymbol{0}$,
- $\boldsymbol{x}_B = [x_B \quad y_B \quad z_B]^{\mathrm{T}}$ is the vector of the offset of the center of buoyancy from the origin of the body-fixed frame of reference wherein the differential equations of the model dynamics are expressed.

A. The IST-ISR Infante

The Infante AUV is a modification of the previous *Marius* prototype AUV built by the Instituto Superior Tecnico in Lisbon, Portugal, [19], [8]. Similarly to the NPS Aries AUV [10], [14], or a theoretical vehicle analysed using FEA[4] [5] it is a chamfered cuboid-shape vehicle with a fined nose-cone, propelled by a pair of aft-mounted thrusters and steered by vertical and horizontal hydrofoils. The Infante, presented in fig. 3 is a relatively large, cumbersome vehicle with a solid potential for carrying scientific payloads into the underwater ocean environment. It is significantly under-actuated and possesses an operational envelope that is significantly constrained by the slow dynamics and holonomic constraints of the kinematic model. The full model dynamics of the Infante utilized in this paper are presented in [22], [20]. The full model dynamics are explored in [22], whereas here we present a summary equations in (7 – **??**), populated with the coefficients in tab. I.

$$\mathbf{M}\dot{\mathbf{x}} = \tau_H + \tau_{prop} + \mathbf{g} \tag{7}$$

$$\tau_H = [X_H\ Y_H\ Z_H\ K_H\ M_H\ N_H]^{\mathrm{T}} \tag{8}$$

$$\tau_{prop} = [\tau_X\ 0\ 0\ \tau_K\ 0\ 0]^{\mathrm{T}} \tag{9}$$

Where $\tau_H \in \mathbb{R}^6$, $\tau_H = [X_H\ \ Y_H\ \ Z_H\ \ K_H\ \ M_H\ \ N_H]^{\mathrm{T}}$ are the hydrodynamical forces and torques on the vehicle, with expressions given in [22], populated by the parameters listed in table I; ρ is the density of salt-water; L is the length of the vehicle; $\tau_{prop} \in \mathbb{R}^6$ are the actuation forces and torques of the vehicle contributed by the vehicle's propellers (the actuation forces and torques contributed by the rudder and the elevators are subsumed in τ_H), with expressions given in [9].

[4]Finite element analysis.

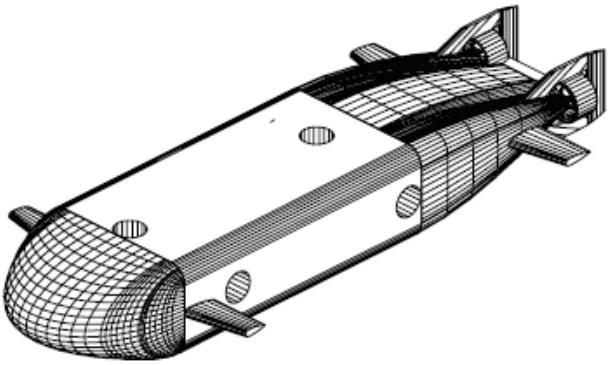

Fig. 2. Infante vehicle operated by the IST-ISR laboratory DSOR.

The values of the dimension-less hydrodynamic coefficients specifying the model dynamics are listed in table I.

TABLE I
PARAMETERS OF INFANTE DYNAMICS.

$m = 2,234.5$ kg	$B = 21,898$N
$I_x = 700$ Nms^2	$I_y = 1,700$ Nms^2
$I_z = 2,000$ Nms^2	$I_{xy} = I_{yz} = I_{zx} = 0$
$x_b = 0.0073$ m	$y_b = 0$ m
$z_b = -0.041$ m	
$\rho = 1,030$ kg/m^3	$L = 4.215$ m
$X_{uu} = -387$	$X_{vv} = -1404$
$X_{ww} = -978$	$X_{\delta b\delta b} = -4,980$
$X_{\delta s\delta s} = -4,980$	$X_{\delta r\delta r} = -878$
$X_{qq} = 5,898$	$X_{rr} = 512$
$X_{w\delta b} = -2,423$	$X_{w\delta s} = -2,423$
$X_{wq} = 355$	$X_{q\delta b} = 633$
$X_{q\delta s} = -801$	$X_{\dot{u}} = -368$
$Y_r = 1,130$	$Y_v = -3,790$
$Y_{rrr} = 3,567$	$Y_{r\|r\|} = -20$
$Y_{v\|v\|} = -7,296$	$Y_{\dot{v}} = -4,448$
$Y_{\dot{r}} = 115$	$Y_{\delta r} = 1,281$
$Z_w = -32,805$	$Z_q = 6,790$
$Z_{\delta b} = -7,539$	$Z_{\delta s} = -7,539$
$Z_{\dot{w}} = -11,973$	$Z_{\dot{q}} = -1,047$
$K_p = -649$	$K_{\delta d} = 3,670$
$K_{\dot{p}} = -25$	
$M_w = 5,476$	$M_q = -3,878$
$M_{\delta b} = 2,411$	$M_{\delta s} = -2,052$
$M_{\dot{w}} = -1,286$	$M_{\dot{q}} = -247$
$N_v = -1,779$	$N_{v\|v\|} = 1,525$
$N_{\delta r} = -690$	$N_r = -878$
$N_{r\|r\|} = -3,800$	$N_{rrr} = -3,891$
$N_{\dot{v}} = 589$	$N_{\dot{r}} = -197$

B. The SSC Pacific CETUS II

The CETUS II is among the few contemporary vehicles that can operate either in a tethered configuration with a fiber-optic data-carrying tether that doesn't provide energy

to the vehicle, effectively becoming an (autonomously powered) ROV, or an untethered, autonomous configuration. Its primary envisaged uses are explosive ordinance disposal, mine countermeasures and search, classify and map missions. CETUS II in use in the SSC[5] Pacific is displayed in figure 4. The control methodology that is used is simple I-P(D) control adopted from [16], [17]. The model dynamics are provided in [7].

Fig. 3. CETUS II vehicle operated by SSC Pacific.

The CETUS II is actuated in all save the sway degree of freedom by joint or differential thrust by 5 thrusters, of which 2 stronger ones, $(T_0,\, T_2)$ are nacelle-mounted off to either side on the stern, and 3 weaker ones $(T_1,\, T_3,\, T_4)$ are in vertical tunnel mountings. The dynamic model, developed through (10 – 13), is taken from [7]. The coefficients are specified in table II.

$$\mathbf{D}(\mathbf{x}) = \mathrm{diag}\{[X_{u|u|}|u|\ Y_{v|v|}|v|\ Z_{w|w|}|w|\ K_{p|p|}|p| \quad \ldots \\ M_{q|q|}|q|\ N_{r|r|}|r|]^{\mathrm{T}}\} \tag{10}$$

$$\mathbf{D} = \mathrm{diag}\{[\ X_u\ \ Y_v\ \ Z_w\ \ K_p\ \ M_q\ \ N_r\ ]^{\mathrm{T}}\} \tag{11}$$

$$\mathbf{T} = \begin{bmatrix} 1 & 0 & 1 & 0 & 0 \\ 0 & 0 & 0 & 0 & 0 \\ 0 & 1 & 0 & 1 & 1 \\ 0 & -L_{ry} & 0 & L_{ry} & 0 \\ 0 & -L_{rx} & 0 & -L_{rx} & L_{fx} \\ L_{by} & 0 & -L_{by} & 0 & 0 \end{bmatrix} \tag{12}$$

$$\begin{aligned} \mathbf{M}\dot{\mathbf{x}} &= -(\mathbf{D}(\mathbf{x}) + \mathbf{D})\mathbf{x} + \boldsymbol{g} + \boldsymbol{\tau}_{prop} \\ &= -(\mathbf{D}(\mathbf{x}) + \mathbf{D})\mathbf{x} + \boldsymbol{g} + \mathbf{T}\boldsymbol{\tau}_{thr} \end{aligned} \tag{13}$$

Where $\boldsymbol{\tau}_{prop} = [\ \tau_X\ \ \tau_Y\ \ \tau_Z\ \ \tau_K\ \ \tau_M\ \ \tau_N\ ]^{\mathrm{T}} = \mathbf{T}\tau_{thr}$ is the vector of actuators' reaction forces and torques, the range of the mapping from the individual thrusters' thrusts to the space spanned by forces and torques supplied by the thruster allocation matrix $\mathbf{T}$, with $\tau_Y \overset{\mathrm{id}}{=} 0$ due to the vehicle's lack of actuation in the sway DOF; $\boldsymbol{\tau}_{thr} = [\ T_0\ \ T_1\ \ T_2\ \ T_3\ \ T_4\ ]^{\mathrm{T}}$ is the vector of thrusts produced by the main, port- and starboard-nacelle-mounted thrusters and the three vertical tunnel thrusters, the assumed *input* of the model. All parameters populating the expressions are listed in table II. It is assumed that the vehicle can be commanded directly in thrust output by the thrusters.

[5]SPAWAR Systems Center.

TABLE II

PARAMETERS OF CETUS II DYNAMICS.

$m = 117.02$ kg	$W = mg = 1,156$ N
$B = 1,152.4437$N	$I_x = 3.37$
$I_y = 45.4984$	$I_z = 30.7391$
$I_{xy} = I_{yz} = I_{zx} = 0$	
$x_b = 0.0073$ m	$y_b = 0$ m
$z_b = -0.0062$ m	$L_{rx} = 0.39$ m
$L_{fx} = 0.565$ m	$L_{ry} = 0.15$ m
$L_{by} = 0.17$ m	
$X_{u\|u\|} = 105.16\ \frac{\mathrm{kg}}{\mathrm{m}}$	$Y_{v\|v\|} = 70.1851\ \frac{\mathrm{kg}}{\mathrm{m}}$
$Z_{w\|w\|} = 165.2648\ \frac{\mathrm{kg}}{\mathrm{m}}$	$K_{p\|p\|} = 0\ \mathrm{kgm}^2$
$M_{q\|q\|} = 0\ \mathrm{kgm}^2$	$N_{r\|r\|} = 0.20\ \mathrm{kgm}^2$
$X_u = 0\ \frac{\mathrm{kg}}{\mathrm{s}}$	$Y_v = 25.6701\ \frac{\mathrm{kg}}{\mathrm{s}}$
$Z_w = 190.0950\ \frac{\mathrm{kg}}{\mathrm{s}}$	$K_p = 0.6598\ \frac{\mathrm{kgm}^2}{\mathrm{s}}$
$M_q = 69.3250\ \frac{\mathrm{kgm}^2}{\mathrm{s}}$	$N_r = 15.525\ \frac{\mathrm{kgm}^2}{\mathrm{s}}$
$\overline{T}_0 = \overline{T}_2 = 102.35$ N	$\overline{T}_1 = \overline{T}_3 = \overline{T}_4 = 53.4$ N

IV. NAVIGATION FEEDBACK AND SOURCES OF ERROR

In order to construct an entire navigation system, the vehicles whose model dynamics were presented in section III need to be equipped with navigation controllers, allowing control of helm or heave speed, or heading or pitch angles. Furthermore, for purposes of realistic simulations, non-stationary noises with statistics of order greater than second must be injected at the appropriate places in the information and signal flow of the feedback systems.

A. Low-Level Controllers

For both vehicles, I-PD controllers which feature feedback linearization in line with [16], [17] were used to navigate the vehicles. The stabilizing action of the implemnted controllers is regulated by the $(K_P,\, K_I)$ coefficients accentuating the action of the proportional and integral channel, respectively, for the I-P controllers, and $(K_P,\, K_I,\, K_D)$ (introducing the coefficient accentuating the action of the derivative channel), for the I-PD controllers. The controllers are listed in table III.

TABLE III

THE DESIGNED FEEDBACK-LINEARIZED I-P(D) CONTROLLERS.

Variable	Type	Param. set
Infante		
Helm speed:	I-P	$(K_{Iu}^{(Inf)},\, K_{Pu}^{(Inf)})$
Heading:	I-PD	$(K_{I\psi}^{(Inf)},\, K_{P\psi}^{(Inf)},\, K_{D\psi}^{(Inf)})$
Pitch angle:	I-PD	$(K_{I\theta}^{(Inf)},\, K_{P\theta}^{(Inf)},\, K_{D\theta}^{(Inf)})$
CETUS II		
Helm speed:	I-P	$(K_{Iu}^{(Cet)},\, K_{Pu}^{(Cet)})$
Heave speed:	I-P	$(K_{Iw}^{(Cet)},\, K_{Pw}^{(Cet)})$
Heading:	I-PD	$(K_{I\psi}^{(Cet)},\, K_{P\psi}^{(Cet)},\, K_{D\psi}^{(Cet)})$

The coefficients are fixed by requiring that the closed-loop transfer function (after cancelation of the nonlinear terms

in the model dynamics) equate to a model Bessel low-pass filter of a matching order. For the I-P controllers (Infante helm speed and CETUS II helm and heave speed) the model function is of 2nd order, so the function is obtained by evaluating for $n = 2$ (14 – 16). For the I-PD controllers (Infante heading and pitch angle and CETUS II heading) the model function is of 3rd order, so (14 – 16) are evaluated for $n = 3$. In (17) the index b_2 is used as a place-holder for any of the states that are controlled by I-P controllers $(u,\, w)$, whereas in (18), the index b_3 is used in lieu of the states controlled by the I-PD controllers $(\theta,\, \psi)$. The symbol I is used as a placeholder of the significant diagonal element of the mass-inertia tensor $\mathbf{M}$ in (4) w.r.t. the degree of freedom (m for $(u,\, w)$ and $(I_y,\, I_z)$ respectively, for $(\theta,\, \psi)$).

$$G_m^{(Bes)} = \frac{\Gamma_n(0)}{\Gamma_n(\frac{s}{\omega_c})} \tag{14}$$

$$\Gamma_n(\frac{s}{\omega_c}) = \sum_{k=0}^{n} a_k \frac{s^k}{\omega_c^k} \tag{15}$$

$$a_k = \frac{(2n-k)!}{2^{n-k}(n-k)!} \tag{16}$$

$$G_{cl}^{(b\,2)} = \frac{1}{\frac{K_P^{(b\,2)}}{K_I^{(b\,2)}I} s^2 + \frac{1}{K_I^{(b\,2)}} s + 1} \tag{17}$$

$$G_{cl}^{(b\,3)} = \frac{1}{\frac{K_P^{(b\,3)}}{K_I^{(b\,3)}I} s^3 + \frac{K_D^{(b\,3)}}{K_I^{(b\,3)}I} s^2 + \frac{1}{K_I^{(b\,3)}} s + 1} \tag{18}$$

The values of $\omega_{c|(u,\theta,\psi)}^{(Inf)}$, the cut-off frequency of the model Butterworth low-pass filters for the helm speed, pitch angle and heading, as well as all values $\{(K_{Iu}^{(Inf)},\, K_{Pu}^{(Inf)}),\, (K_{I\psi}^{(Inf)},\, K_{P\psi}^{(Inf)},\, K_{D\psi}^{(Inf)}), \ldots$ $(K_{I\theta}^{(Inf)}, K_{P\theta}^{(Inf)},\, K_{D\theta}^{(Inf)})\}$ for the Infante AUV are given in tab. IV. Likewise, the $\omega_{c|(u,w,\psi)}^{(Cet)}$ and all values $\{(K_{Iu}^{(Cet)},\, K_{Pu}^{(Cet)}),\, (K_{Iw}^{(Cet)},\, K_{Pw}^{(Cet)}), \ldots$ $(K_{I\psi}^{(Cet)},\, K_{P\psi}^{(Cet)},\, K_{D\psi}^{(Cet)})\}$ for the CETUS II are given in tab. V.

TABLE IV

THE VALUES OF THE LOW-LEVEL CONTROLLER PARAMETERS FOR INFANTE.

Helm speed	
$\omega_{c\|u}^{(Inf)} = 0.55$ rad/s	
$K_{Iu}^{(Inf)} = 675.936$	$K_{Pu}^{(Inf)} = 2.129 \cdot 10^3$
Heading	
$\omega_{c\|\psi}^{(Inf)} = 0.25$ rad/s	
$K_{I\psi}^{(Inf)} = 125$	$K_{P\psi}^{(Inf)} = 125$
$K_{D\psi}^{(Inf)} = 866.025$	
Pitch angle	
$\omega_{c\|\theta}^{(Inf)} = 0.25$ rad/s	
$K_{I\theta}^{(Inf)} = 125$	$K_{P\theta}^{(Inf)} = 125$
$K_{D\theta}^{(Inf)} = 866.025$	

TABLE V

THE VALUES OF THE LOW-LEVEL CONTROLLER PARAMETERS FOR CETUS II.

Helm speed	
$\omega_{c\|u}^{(Cet)} = 2.8$ rad/s	
$K_{Iu}^{(Cet)} = 917.4368$	$K_{Pu}^{(Cet)} = 567.5168$
Heave speed	
$\omega_{c\|w}^{(Cet)} = 5.6$ rad/s	
$K_{Iw}^{(Cet)} = 3.670 \cdot 10^3$	$K_{Pw}^{(Cet)} = 1.135 \cdot 10^3$
Heading	
$\omega_{c\|\psi}^{(Cet)} = 0.8$ rad/s	
$K_{I\psi}^{(Cet)} = 15.7384$	$K_{P\psi}^{(Cet)} = 48.5178$
$K_{D\psi}^{(Cet)} = 59.8277$	

B. Noise Generators

The simulation of the navigation of both vehicles must feature realistic and non-trivial process and measurement noise. The additive terms of *process noise* introduced in the expression for $\dot{\mathbf{x}}$ will simulate the effects of the limits of accuracy of the model dynamics in describing the actual physical system. All parameters of the process and measurement noise statistics and generators presented heretofore are taken from [2].

a) Process noise.: It follows from operational experience that correlated and rate-limited multi-dimensional Gaussian noise models the lack of trustworthiness of the model dynamics, and the appearance of stochastic environmental disturbances sufficiently well.

b) Measurement noise.: The measurement noise as well should mimic the fieldwork experience of AUV operations. From experience, the operation of sensors produces errors in the readings whose sources cannot be simply identified by recourse to first-order statistics. To emulate this, measurement errors cannot be stationary, zero-mean, nor completely described by first-order statistics. Additionally, a mechanism should be provided to generate *sporadic faults* in each measurement channel. An example of such a fault is *loss of bottom-lock* of a DVL transducer. Therefore, a process noise generator based on *Hidden Markov Models* [21], [6], [27] is proposed.

The process noise generator uses a bank of 10 HMMs, as per [2]. Out of these, 7 HMMs are used to generate the noise added to each of the directly measured states $[\ \boldsymbol{u}_m(k)^{\mathrm{T}}\ \ \boldsymbol{\Theta}_m(k)^{\mathrm{T}}\ \ z_m(k)\ ]^{\mathrm{T}}$. The remaining 3 are used to generate the additive noise to the position of the transponder, $\delta \boldsymbol{b}_{usbl}$. The states of HMMs generating the noises $(\delta\phi,\, \delta\theta,\, \delta\psi)$ are *univariate rate-limited von Misen noise generators* [1], [3], [11]. To optimize for a realistic nature of the measurement noises and, each of the 10 HMMs contains 6 states, {*nominal, +reliable, -reliable, +unreliable, -unreliable,fault*}.

According to type, the HMMs of the process noise generator are divided into 7 *Gaussian Markov models* (for u_m, v_m, w_m, x_{usbl}, y_{usbl}, z_{usbl}, z_m), and 3 *Von Mises Markov models*, generating the noise in *angular measure-*

ment channels.

V. SIMULATION STUDIES

In this section, the results of simulated navigation experiments with both the IST-ISR Infante vehicle, and the SSC Pacific CETUS II are performed. The simulations use in-depth model dynamics of the vehicles briefly summarized in sec. III and further developed in [22], [7], for the Infante and CETUS II, respectively. The simulations use the low-level controllers designed in sec. IV.A and the noise generators designed in sec. IV.B.

The simulations consist of a composite maneuver that excites all provided command channels for the individual vehicle. The profile for both vehicles is the same, whereas the scale, i.e. the actual required commands, in terms of the dynamics required of vehicles, differ due to the physical sized, installed motive power and dynamic and holonomic constraints. The composite maneuver consists of an initial straight-line cruise whilst accelerating to nominal helm speed, followed by a heading change towards East. On the cruise leg stretching in the East direction, a depth-change maneuver is executed. The nature of the maneuver differs, since Infante dives by pitching down and progressing forward, whereas the CETUS II dives by engaging all three of its vertical tunnel thrusters that collaboratively change its heave speed and dive or surface the vehicle. After the completed depth change maneuver, both vehicles are commanded to come back on the pure northerly course.

A. Simulation of Infante Navigation

The simulated model of the Infante, with the process and measurement noise injected, was simulated to cruise along a trajectory produced by the command signals for the low level controllers that are displayed in figs. 5 – 7 in magenta dotted lines.

The navigation SP-UK-filter, working during the execution of the maneuver displayed in figure 8, produced the estimates for $\hat{\boldsymbol{u}} = [\hat{u} \;\; \hat{v} \;\; \hat{w}]^{\mathrm{T}}$ in figure 5, for $\hat{\boldsymbol{\omega}} = [\hat{p} \;\; \hat{q} \;\; \hat{r}]^{\mathrm{T}}$ in figure 6, and for the attitude, $\hat{\boldsymbol{\Theta}} = [\hat{\phi} \;\; \hat{\theta} \;\; \hat{\psi}]^{\mathrm{T}}$ in figure 7.

B. Simulation of SSC Pacific CETUS II

The simulated model of the CETUS II, with the process and measurement noise injected, was simulated to cruise along a trajectory produced by the command signals for the low level controllers that are displayed in figs. 9 – 11 in magenta dotted lines.

The navigation SP-UK-filter, working during the execution of the maneuver displayed in figure 12, produced the estimates for $\hat{\boldsymbol{u}} = [\hat{u} \;\; \hat{v} \;\; \hat{w}]^{\mathrm{T}}$ in figure 9, for $\hat{\boldsymbol{\omega}} = [\hat{p} \;\; \hat{q} \;\; \hat{r}]^{\mathrm{T}}$ in figure 10, and for the attitude, $\hat{\boldsymbol{\Theta}} = [\hat{\phi} \;\; \hat{\theta} \;\; \hat{\psi}]^{\mathrm{T}}$ in figure 11.

VI. CONCLUSIONS

In this paper, the simulation analysis of the effectiveness, robustness and accuracy of the Unscented Kalman filter [24] was performed. The analysis was broadened in scope by considering two significantly different, yet practically

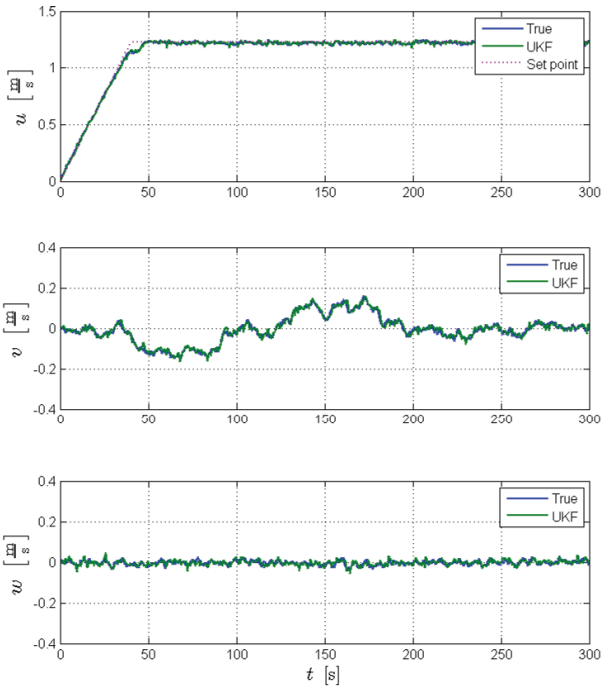

Fig. 4. The comparison of the original (incl. process noise) and SP-UK-filtered estimates of the $(\hat{u}, \hat{v}, \hat{w})$ – linear 3D speed-over-ground states based on the DVL measurements during the simulated composite maneuver of the Infante model dynamics presented in fig. 8.

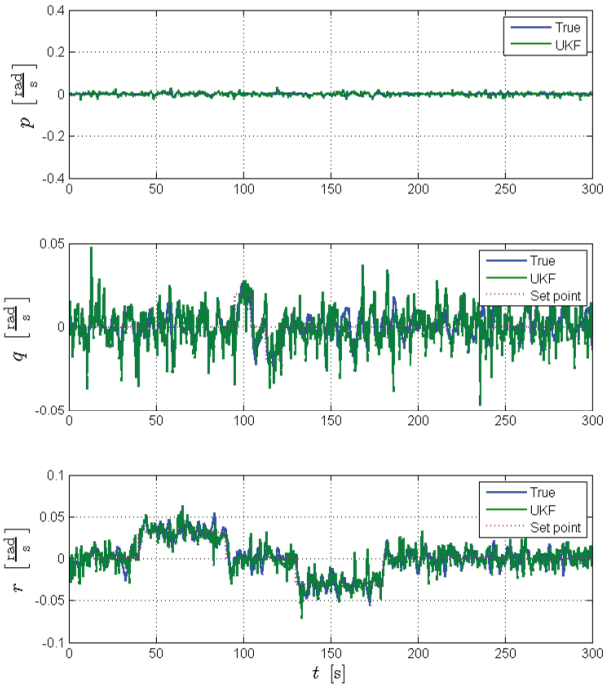

Fig. 5. The angular rates of rotation $(\hat{p}, \hat{q}, \hat{r})$ estimated by the SP-UKF using the Infante model dynamics during a maneuver presented in fig. 8.

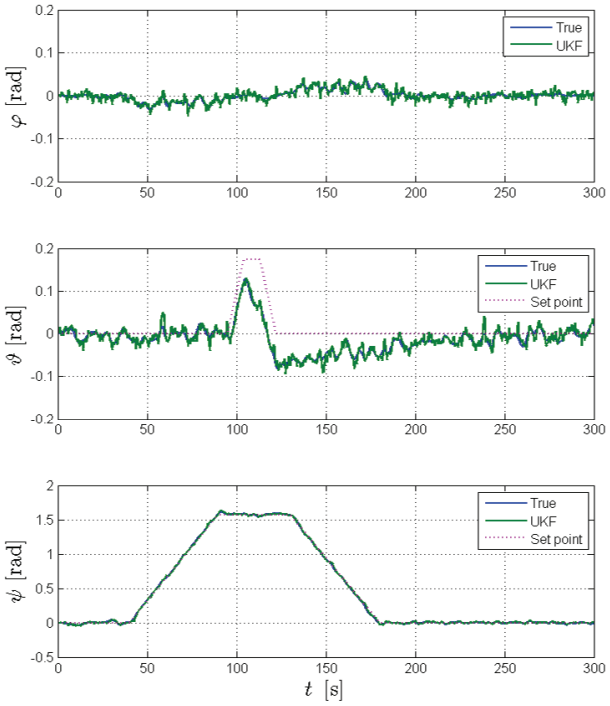

Fig. 6. The comparison of the original (incl. process noise) and SP-UKF-filtered estimates of $(\hat{\phi}, \hat{\theta}, \hat{\psi})$ – the attitude Euler angles, based on the strapdown AHRS measurements during the simulated composite maneuver of the Infante model dynamics presented in fig. 8.

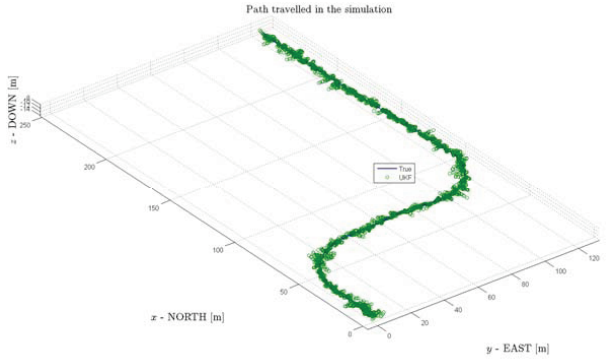

Fig. 7. The *SP-UKF* navigation filter acting through a simulated composite maneuver of the Infante model dynamics.

representative vehicles, with substantively different model dynamics, kinematics and thrust allocation. The analysis was further enhanced in relevance and realism by including detailed, non-linear models of the vehicles in low-level control loops that feature simple, I-PD controllers designed with recourse to simplified, decoupled models. Furthermore, a precise mechanism of simulating the hydroacoustic localization low-level signals (time delays) on the inverse-USBL transducer array assumed to be mounted on both vehicles was included.

A realistic, Gaussian rate-limited and coupled model of process noise and a non-stationary model of measurement noise based on stochastic state machines (Hidden Markov

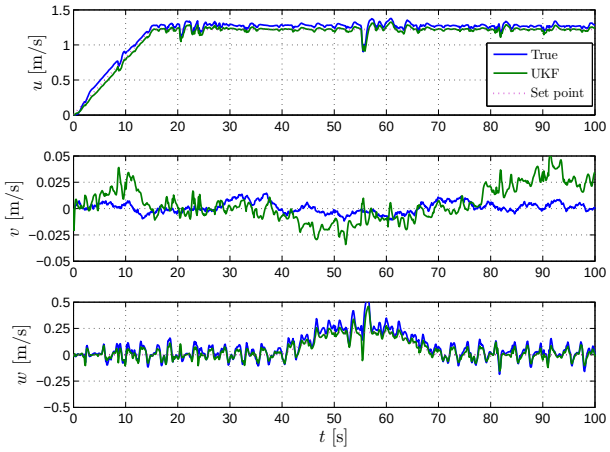

Fig. 8. The comparison of the original (incl. process noise) and SP-UKF-filtered estimates of the $(\hat{u}, \hat{v}, \hat{w})$ – linear 3D speed-over-ground states based on the DVL measurements during the simulated composite maneuver of the CETUS II model dynamics presented in fig. 12.

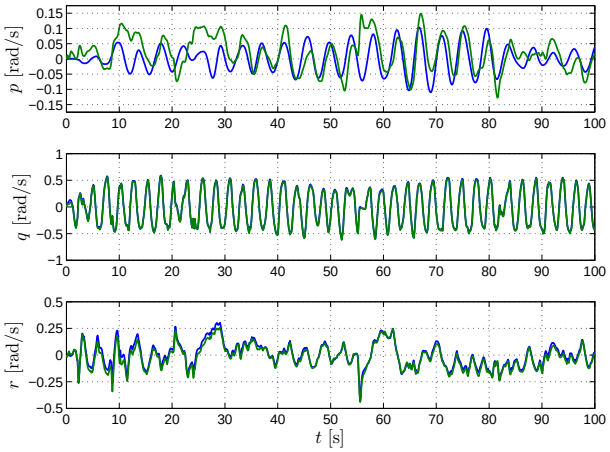

Fig. 9. The angular rates of rotation $(\hat{p}, \hat{q}, \hat{r})$ estimated by the SP-UKF using the CETUS II model dynamics during a maneuver presented in fig. 12.

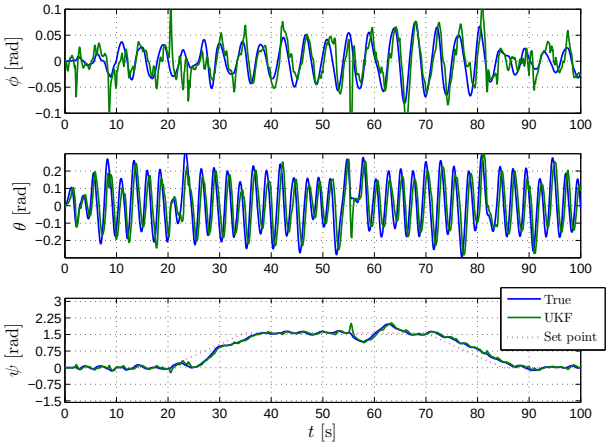

Fig. 10. The comparison of the original (incl. process noise) and SP-UKF-filtered estimates of $(\hat{\phi}, \hat{\theta}, \hat{\psi})$ – the attitude Euler angles, based on the strapdown AHRS measurements during the simulated composite maneuver of the CETUS II model dynamics presented in fig. 12.

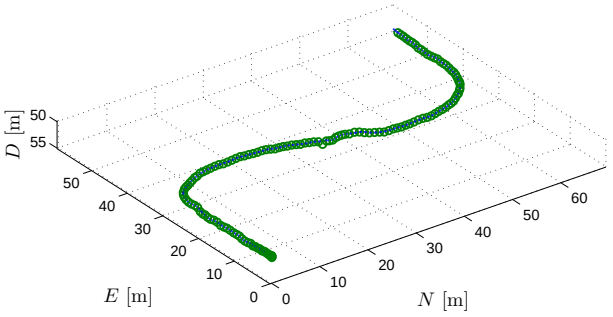

Fig. 11. The *SP-UKF* navigation filter acting through a simulated composite maneuver of the CETUS II model dynamics.

models) were developed to lend credulity to the simulation analysis and mimic real-world operational conditions as well as possible. An interpolating median prefilter, an outlier rejector and a post-processing 1st order Bessel smoother were all chained with the primary, SP-UKF navigation block to make the navigation fixing more robust and stable in the presence of outliers and intermittent failures in obtaining navigation measurements.

The Unscented Kalman filter methodology was shown to allow for stable and robust navigation via low-level control loop closing. The feedback loops closed using the outports of the navigation filter were used effectively for navigation using the designed linear controllers.

A. Further Works

The Scaled Unscented Transform Sigma-point Kalman Filter presented herein will be developed, implemented and commissioned aboard the embedded control systems of the *PlaDyPos* autonomous surface platform, the *Seamor F300* ROV and the *Iver 2* AUV operated by LABUST[6].

REFERENCES

[1] M. Abramowitz and I.A. Stegun. *Handbook of mathematical functions with formulas, graphs, and mathematical tables*. Number v. 55, no. 1972 in Applied mathematics series. U.S. Govt. Print. Off., 1964.

[2] Matko Barisic. *Guidance Of Formations Of Autonomous Underwater Vehicles By Virtual Potential Method*. PhD thesis, University of Zagreb, Faculty of Electrical Engineering and Computing, Unska 3, Zagreb, Croatia, mar. 2012.

[3] D. J. Best and N. I. Fisher. Efficient simulation of the von Mises distribution. *Journal of the Royal Statistical Society. Series C (Applied Statistics)*, 28(2):152 –157, 1979.

[4] Richard Bildberg. Editor's foreword. In Bildberg R., editor, *Proceedings of the 16th International Symposium on Unmanned Untethered Submersibles Technology*. Autonomous Undersea Systems Institute, August 2009. on CD.

[5] R.J. Boncal. A Study of Model Based Maneuvering Controls for Autonomous Underwater Vehicles. Master's thesis, Naval Postgraduate School Monterey CA USA, dec 1987.

[6] Roger D. Boyd. Hidden Markov Models: An online tutorial. Technical report, University of Leeds, Faculty of Engineering, School of Computing, School of Computing, University of Leeds, Leeds LS2 9JT, UK.

[7] V. Djapic. *Unifying Behavior Based Control Design and Hybrid Stability Theory for AUV Application*. PhD thesis, University of California Riverside CA, USA, mar. 2009.

[6]The Laboratory for Underwater Systems and Technologies, University of Zagreb, Faculty of Electrical Engineering and Computing.

[8] P. Egeskov, A. Bjerrum, A. Pascoal, C. Silvestre, C. Aage, and L.W. Smitt. Design, construction and hydrodynamic testing of the auv marius. In *Autonomous Underwater Vehicle Technology, 1994. AUV '94., Proceedings of the 1994 Symposium on*, pages 199 –207, jul 1994.

[9] S.A. Harvald. *Resistance and propulsion of ships*. Ocean engineering. John Wiley & Sons, 1983.

[10] A.J. Healey and D. Lienard. Multivariable sliding mode control for autonomous diving and steering of unmanned underwater vehicles. *Oceanic Engineering IEEE Journal of*, 18(3):327 –339, jul 1993.

[11] S.R. Jammalamadaka and A. Sengupta. *Topics in circular statistics*. Series on multivariate analysis. World Scientific, 2001.

[12] R.E. Kalman. On the general theory of control systems. *Automatic Control, IRE Transactions on*, 4(3):110, dec 1959.

[13] R.E. Kalman. A new approach to linear filtering and prediction problems. *Transactions of the ASME, Journal of Basic Engineering*, pages 35–45, mar 1960.

[14] D.B. Marco and A.J. Healey. Command control and navigation experimental results with the NPS Aries AUV. *IEEE Journal of Oceanic Engineering*, 26(4):466–476, 2001.

[15] 3DM-GX1 Gyro Enhanced Orientation Sensor, Datasheet of the. `http://www.microstrain.com/pdf/3DM-GX1%20Datasheet%20Rev%201.pdf`, 2010.

[16] Nikola Miskovic, Dula Nad, and Zoran Vukic. 3D Line Following for Unmanned Underwater Vehicles. *Brodogradnja / Shipbuilding: Croatian Journal of Naval Architecture and Shipbuilding Industry*, 61(2):121–129, 2010.

[17] Nikola Miskovic, Zoran Vukic, Marco Bibuli, Gabriele Bruzzone, and Massimo Caccia. Fast in-field identification of unmanned marine vehicles. *Journal of Field Robotics*, 28(1):101–120, 2011.

[18] M. Morgado, P. Oliveira, and C. Silvestre. Design and experimental evaluation of an integrated usbl/ins system for auvs. In *Robotics and Automation (ICRA), 2010 IEEE International Conference on*, pages 4264 –4269, may 2010.

[19] A. Pascoal, P. Oliveira, C. Silvestre, A. Bjerrum, A. Ishoy, J.-P. Pignon, G. Ayela, and C. Petzelt. Marius: an autonomous underwater vehicle for coastal oceanography. *Robotics Automation Magazine, IEEE*, 4(4):46 –59, dec 1997.

[20] N. Paulino, C. Silvestre, R. Cunha, and A. Pascoal. A bottom-following preview controller for autonomous underwater vehicles. In *Decision and Control, 2006 45th IEEE Conference on*, pages 715 – 720, dec. 2006.

[21] L. R. Rabiner and B. H. Juang. An introduction to hidden Markov models. *IEEE ASSP Magazine*, pages 4–15, January 1986.

[22] Carlos Silvestre and Antonio Pascoal. Infante AUV dynamic model. Technical report, Institute for Systems and Robotics, Instituto Superior Tecnico, Lisbon, Portugal, oct. 2001. DSORL-ISR/IST Technical report.

[23] Teledyne RD Instruments Phased Array Velocity Sensor (PAVS), Datasheet of the. `http://www.rdinstruments.com/PAVS.aspx`, 2011.

[24] R. van der Merwe. *Sigma-Point Kalman Filters for Probabilistic Inference in Dynamic State-Space Models*. PhD thesis, OGI School of Science & Engineering, Oregon Health & Science University, Portland OR USA, apr. 2004.

[25] K. Vickery. Acoustic positioning systems. new concepts-the future. In *Autonomous Underwater Vehicles, 1998. AUV'98. Proceedings Of The 1998 Workshop on*, pages 103 –110, aug 1998.

[26] N. Wiener. *Extrapolation, interpolation, and smoothing of stationary time series: with engineering applications*. Technology press books in science and engineering. Technology Press of the Massachusetts Institute of Technology, 1949.

[27] W. Zucchini and I.L. MacDonald. *Hidden Markov models for time series: an introduction using R*. Monographs on statistics and applied probability. CRC Press, 2009.